Characterizing Photodiodes of the Homodyne Detector for Advanced Virgo Squeezer

Alexandra Montesano

August 1, 2017

Contents

1 Abstract

In the process for squeezing light, the homodyne detector is the device that detects the level of squeezing in a given method. In 2015, the squeezing group at La Sapienza developed a circuit board for the homodyne detector. In this report, I summarize the measurements done on the on the homodyne detector to verify how the DC response of the photodiode (PD) changes in function of the angle of incidence (AOI) and the polarization of the incoming beam in two different configurations. The purpose of these tests is to discover under what conditions the PDs produce the maximum DC Voltage.

2 Introduction

2.1 Gravitational Waves

Gravitational Waves (GW) are very relevant in physics today. It started with Einstein's prediction that there are changes in spacetime that are caused by large cosmic interactions [7]. In the past two years, scientists have detected three GWs. Though all of these detections were caused by "violent" interactions in space, any accelerating mass can, in theory, produce gravitational radiation. The problem is that the detectors that exist today are not sensitive enough to observe smaller interactions. Around the world there are four major gravitational wave detectors, including two LIGO observatories located in the United States, Virgo located in Italy, and GEO600 located in Germany. To make an accurate observation of GWs, there must be detection from at least three of the four sites.

Virgo was constructed as a Michaelson Interferometer with three kilometer long arms to detect GWs. Since its original construction in 2003, Virgo has been modified from its original design. In 2011, Virgo began to undergo a series of upgrades to increase sensitivity, becoming Advanced Virgo. Since then, Virgo has gone through many scientific runs and continues its

journey to increase sensitivity for the detection of GWs in the future.

2.2 Motivation

The ultimate goal of squeezed light in this context is to reduce the quantum noise found in GW detectors. La Sapienza University of Rome is a section of the National Institute of Nuclear Physics, one of the main collaborators in the construction of Virgo. Facing the problem of sensitivity in Virgo, at La Sapienza they are exploring using squeezed light to combat this issue. There is already a method of squeezing being explored in the Squeezing Lab to improve sensitivity; this is the Optical Parametric Oscillator based method. With this method in other detectors, there has been progress in improving detection; however the group at La Sapienza believes the Ponderomotive Squeezing of Light could be more successful. The goal of the POLIS (**Po**nderomotive **Li**ght **S**queezing) project is to improve sensitivity in the low frequency band. This is a deficiency found in other squeezing methods.

Currently, the INFN section at La Sapienza has provided the circuit board for the Homodyne Detector in the Squeezing Lab at Virgo. An Optical Parametric Oscillator system is used to produce the squeezed light. The PD used in conjunction with this circuit is a custom made, high efficiency Infrared PD from LASER COMPONENTS ® (LC). The manufacturer gave us the information that the PDs have a maximum response at an AOI of 20° with an incoming beam of S-Polarization; however, this was not confirmed experimentally. There is also uncertainty on which axis the detector should be rotated. With the present work, we wanted to check experimentally these PD characteristics. It is necessary to find the maximum DC Output Voltage, so that it is certain we are maximizing the functionality of the PD. The Eptiaxx PDs were used to perfect the experimental procedure before taking data with the LC PDs. The homodyne detector used will also be the same for the experimental setup for the Ponderomotive method of light squeezing. We used the homodyne detector to test these features because it already has a

DC Output channel for both PD positions; this allows us to observe the changes in the voltage without requiring new electronics.

3 Squeezed Light

3.1 Quantum Noise in Advanced Detectors

Because these advanced detectors have increased sensitivity, their main limitation is the quantum nature of light. The sources of noise in these detectors are shown in *Figue 1*, where you can see the noise of Advanced Virgo (AdV) is approaching this limit. The Quantum Noise is an uncorrelated sum of both the Radiation Pressure Noise and the Shot Noise:

$$h_{quantum}(v) = \sqrt{h^2_{shot}(v) + h^2_{RP}(v)}$$

The Radiation Pressure Noise (RPN) is due to the transfer of momentum from the photons to the mirrors where as the Shot Noise (SN) is due to the uncertainty in the number of photons. RPN dominates the quantum noise at low frequencies and S.N. at high frequencies. Squeezed States of Light are seen as a solution to overcoming the Standard Quantum Limit. Light can be squeezed in one of two quadrature, each of which correspond to one of the contributions to the quantum noise. As seen in *Figure 2*, the uncertainties in both quadrature obey the Heisenberg Uncertainty Principle. We cannot defy this, but we can minimize the uncertainty in one quadrature to generate a squeezed state. An ideal squeezer would produce frequency dependent squeezed states to overcome many values of RPN and SN across the GW detection spectrum.

3.2 OPO Squeezing

Optical Parametric Oscilator based squeezing utilizes the characteristics of non-linear crystals and mirrors in a cavity to produce squeezed states. This method is currently being explored at Virgo and has shown success at GEO600 in Hannover. This method of squeezing requires two

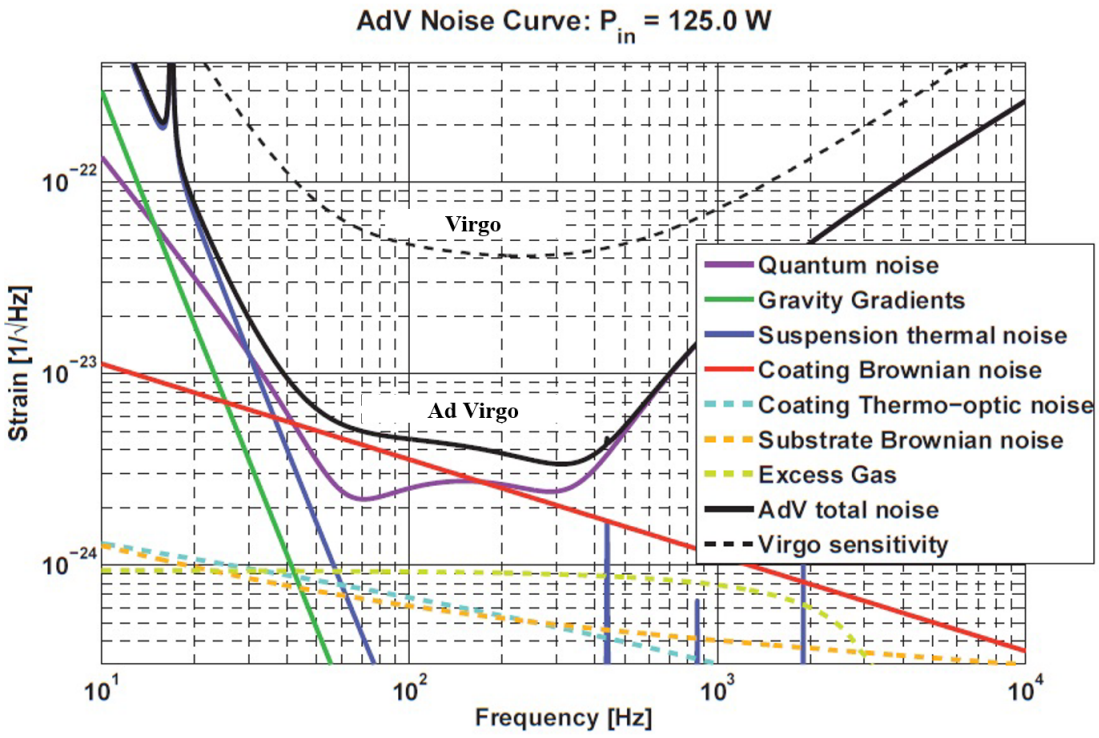

Figure 1: This figure is a graphical representation of the expected noise sources of AdV. [3]

$$\langle(\Delta\hat{X}_1)^2\rangle\langle(\Delta\hat{X}_2)^2\rangle \geq \frac{1}{16}$$

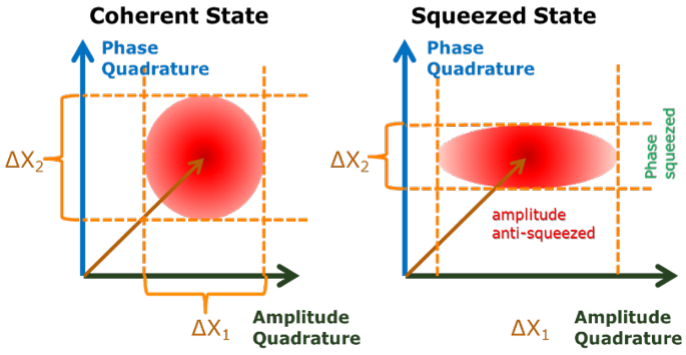

Figure 2: This figure shows the effect of squeezing on the Phase Quadrature as well as the equation defining the uncertainties in both quadratures by the Heisenberg Uncertainty Principal. [3]

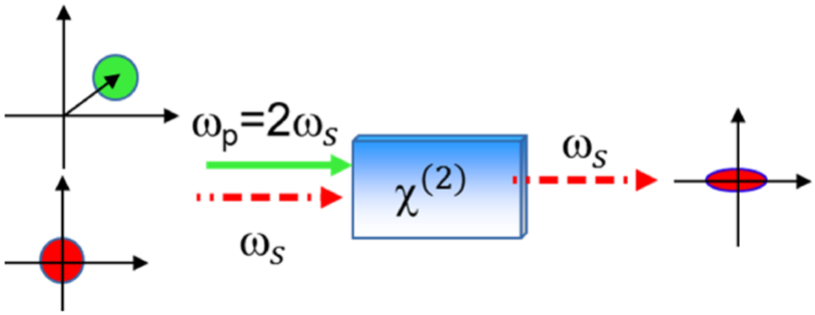

Figure 3: This figure shows method of producing squeezed light with non-linear crystals. [6]

lasers one with a frequency of ω_0 and one with a frequency of $2\omega_0$, as shown in *Figure 3*. The combination of these two lasers with the non-linear processes in the dielectric generate a phase quadrature squeezed state. This makes OPO Squeezing very effective in reducing Shot Noise at high frequencies; however a method is needed to reduce RPN at lower frequencies.

3.3 Ponderomotive Squeezing

Ponderomotive Squeezing is a method that uses the features of optical springs in an empty cavity with suspended mirrors to produce squeezed light. The effects of the optical springs have been observed; however there is yet a group to observe squeezed states with this method. It is being pursued because of it's potential to produce frequency dependent squeezed states. As seen in *Figure 4*, the squeezed state is produced by the radiation pressure creating a phase shift between the two mirrors that couples the phase and amplitude quadratures. The Light Squeezing group at La Sapienza is working to construct a suspended bench for producing this method of squeezing.

4 Homodyne Detection

The Homodyne Detector is composed of a circuit board that has five channels and two PDs. It is used as a diagnostic tool in measuring the amount of squeezed light produced in a given system.

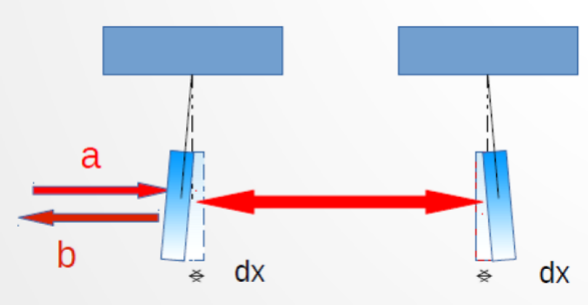

Figure 4: This figure shows method of producing squeezed light with an empty cavity containing suspended mirrors. [4]

A conceptual scheme of the circuit can be found in *Figure 5*. The "Self-Subtraction" allows us to

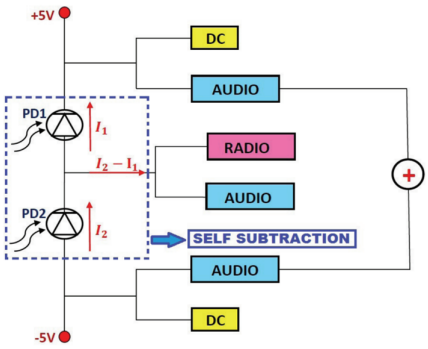

Figure 5: This figure shows an conceptual scheme of the functions of the electronics on the Homodyne Detector [2].

gain information on the squeezed light produced where the "Sum" gives information regarding the shot noise of the local oscillator [2] Our interest in the Homodyne Detector is for the use of it's DC Outputs. This circuit provides us with a convenient way to measure the DC signal produced by the PDs without having to introduce new electronics.

A picture of the Homodyne Circuit that is used both in the lab at La Sapienza and at Virgo is shown in *Figure 6*. Connections were made to the homodyne detector for measuring the DC Voltage Output of each PD as shown in *Figure 7*. We use the oscilloscopes to measure the DC signal of either PD, and the DC Voltage Source is used to aliment the circuit and thus the PDs.

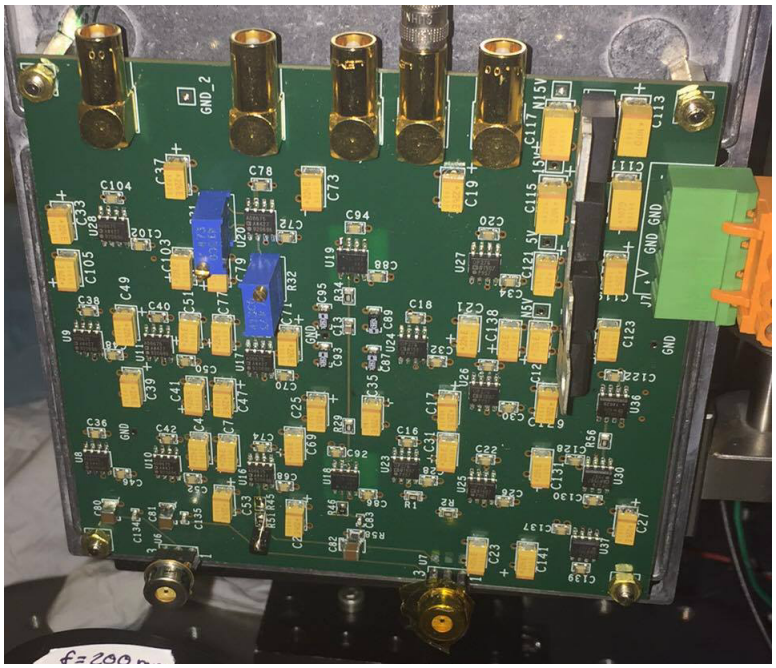

Figure 6: This figure shows an image of the homodyne detector used for experiments at La Sapienza and Virgo.

5 Gaussian Beam Characteristics

A Nd:YAG, 1064nm, Gaussian beam laser was used to generate the photocurrent in the homodyne detector. The beam has a Guassian profile meaning it does not have a constant radius as shown in *Figure 8*. The smallest radius of the beam is called the beam waist (w_0). Then the beam expands as you travelling farther from the waist. The rate at which the beam grows after the waist is represented by the divergence in the following equation:

$$\theta = \lambda/(\pi w_0)$$

. Other values related to the Gaussian beam are the Rayleigh Range (z_r), the Depth of Focus (b), and the Beam Radius as a Function of Distance (w(z)), where "z" represents the position on the optical axis. As you add lenses in the path of the Gaussian beam, all the aforementioned values are distorted from those of the original beam. To model this, we have used a program

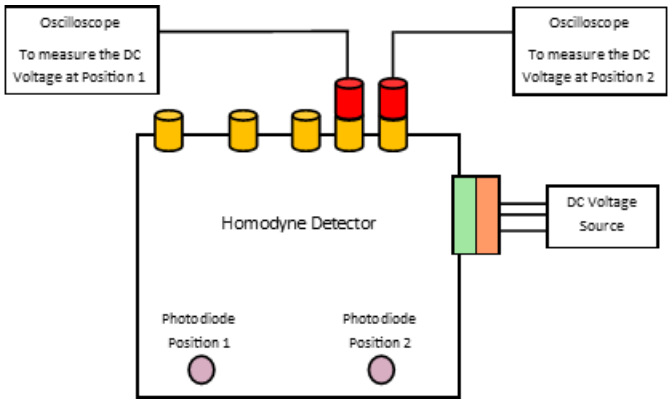

Figure 7: This figure shows a diagram of the connections made to the homodyne detector to measure the DC Voltage Output of either PD.

called GaussianBeam to simulate the effects of optical elements on the beam (this will be further discussed in Section-Method-)

6 Experimental Method

6.1 Gaussian Beam Simulation

Before taking data, we had to design an optical path that would keep the Gaussian Beam waist smaller than the PD's sensitive area. To assist in modelling the behavior of the Gaussian Beam through different optical elements, we used the program "GaussianBeam." We found that the optimal configuration was that shown in *Figure 9*. This decision was based on obtaining the best beam waist size and position while using lenses that were available to us in the lab. Moreover, we wanted to have a beam with a small divergence, so the waist does not vary much when the AOI is shifted. To compensate for any divergence we will move the homodyne and thus the PD along the optical axis, so that the PD will not be always at the beam waist position.

After configuring the path of the beam, we took a few days to finalize the setup. We decided that three translation stages in the x-y-z planes would be ideal for realigning of the homodyne detector after adjustments were made with a rotation stage. Our biggest challenge was finding

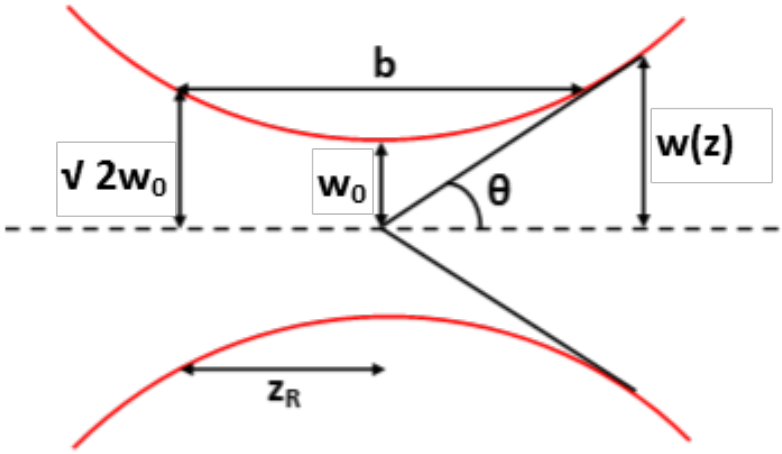

Figure 8: This figure shows a diagram of a Gaussian Beams with the relevant parameters.

compatible stages to create a stable stand for the detector. A complete list of equipment used in the optical setup can be found in *Appendix I*.

6.2 Rotation θ_y

The first set of data was taken to check the beam polarization. To do this we had to put two optical densities just after the laser to attenuate the out-coming power from the laser. The power meter that we use for these measurements has a maximum power of 5mW, beyond this threshold it saturates. We did not change the polarization for the original set of measurements. Another set of measurements was taken to understand if the waveplates available in the lab were quarter waveplates (QWP) or half wave plate (HWP). We needed this information in order to manipulate the polarization of the laser beam arriving on our detector. We know that the beam produced by the laser has a defined polarization S, but we need 1 HWP or a combination of 2 QWP to change the polarization from S to P. In addition along the beam path, after the two optical densities (ODs), we put a polarizing beam splitter (PBS) in order to ”clean” the polarization of the beam. In fact, the beam produced by the laser is not a purely S-Polarized, but it has a small contribution of P polarization; more precisely the beam was 90% S-Polarized

Optics	Position (mm)	Relative position (mm)	Properties	Waist (µm)	Waist position (mm)	Rayleigh range (mm)	Divergence (mrad)	Sensitivity (%/mm²)	Name	Lock
Input be...	-90		n = 1, M² ...	145	-90	62.0789	2.33573	0.00648712	w0	absol...
Lens	100	190	f = 125 mm	201.653	350.715	120.065	1.67953	0.0079131	L1	none
Lens	300	200	f = 200 mm	145.084	370.22	62.1507	2.33438	0.00400588	L2	none

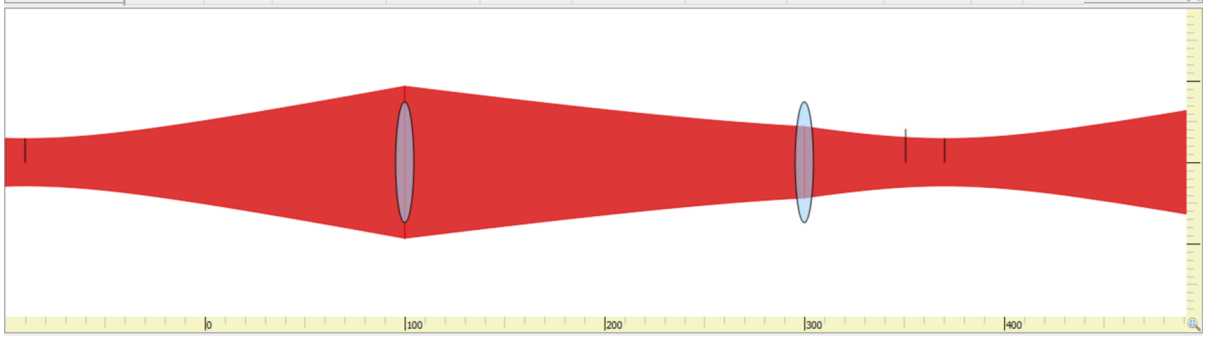

Figure 9: This figure shows the optimized parameters of the optical elements to be set-up on the optical bench in order to fit previous constraints. This work was done using GaussianBeam® software.

and 10% P-Polarized. The PBS allowed us to split the two contributions and be sure of the polarization of the beam arriving on the detector. To accommodate the limits of our power meter, we switched out the two optical densities for a stronger filter. We found that we could produce 98% S-Polarized light with the first polarizer at 28° and the second at 50°. This became the S-Polarized configuration for the following measurements. We found that with the first polarizer at 28° and the second at 185° we could produced 94% P-Polarized light. This became the P-Polarized configuration for the following measurements.

With thee variation in the polarization of the beam, we took data manipulating the AOI of the laser on the PD of the homodyne detector for each polarization. A schematic of this setup is shown in *Figure 10*. This setup can be manipulated to also measure the S-Polarized light by moving the second lens and adjusting the quarter wave plates. With these configurations we adjusted the AOI around the y-axis using the rotational stage. We then used the x-y-z translation stages to realign the beam on the PD. The alignment is complete when the DC signal is maximized. This will be referred to as *Rotation* θ_y and can be seen in *Figure 11*. After taking

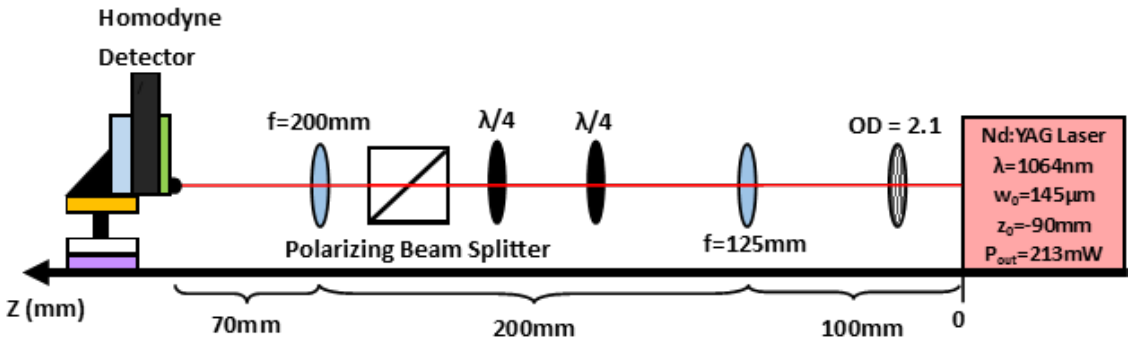

Figure 10: This figure shows a schematic for the setup required to measure the DC Output Voltage versus the AOI of the homodyne detector with P-Polarized light.

data with the Eptiaxx PD and perfecting the experimental procedure, we switched it out for the LC #1 and #4 PD. We tested the DC Voltage Output dependence on polarization and AOI again for these PD.

6.3 Rotation θ_x

We had inferred that our results would be the same regardless of the plane in which we rotated the detector; however, we wanted to confirm this hypothesis. We spent another day reconfiguring the base of the homodyne detector to rotate around the x-axis as shown in *Figure 12*. This new configuration allowed us to rotate on the new axis as well as adjust the homodyne detector in the x-y-z plane for realignment. For this configuration, we used a similar experimental procedure to measure the DC Voltage Output—use the rotational stage to set the AOI and adjust the x, y, and z stages to find the maximum DC signal. This will be known as *Rotation* θ_x. For this set of data we also tested the effect of the direction of rotation on the DC Voltage Output under the hypothesis that it would not affect the DC signal. We rotated the detector about the x-axis in both the clockwise and counterclockwise directions. We were unable to rotate in both directions for Rotation θ_y because of the physical limits of the optical bench.

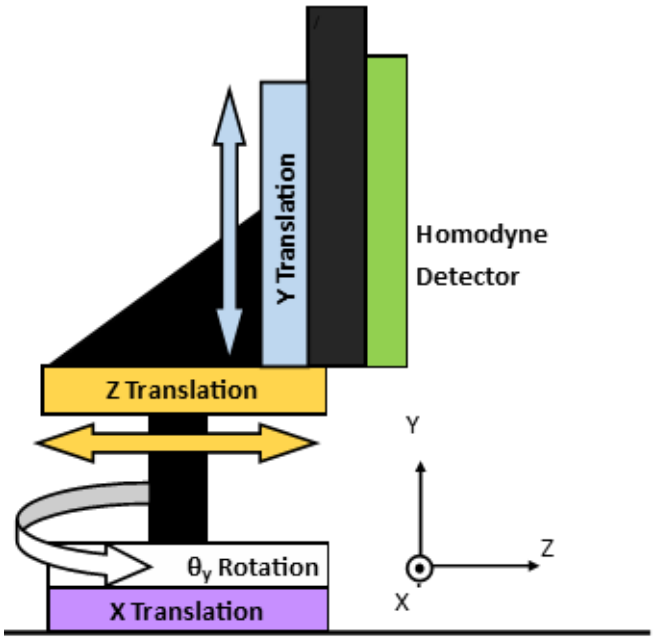

Figure 11: This figure shows a schematic for rotating the homodyne detector about the y-axis.

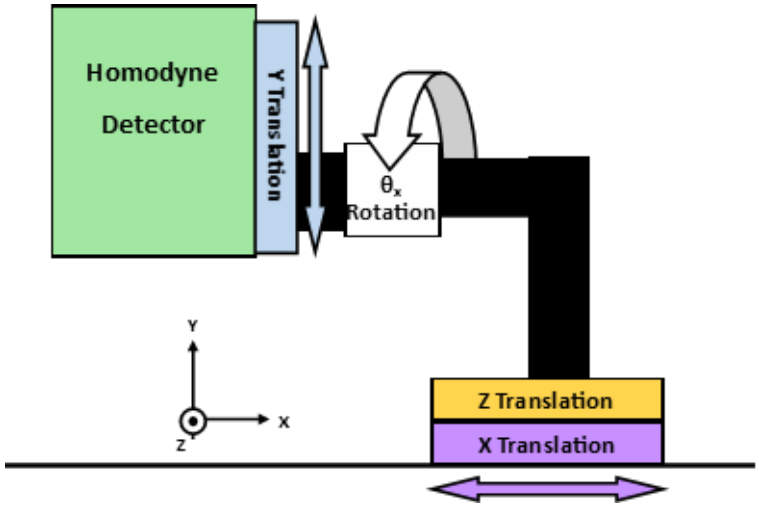

Figure 12: This figure shows a schematic for rotating the homodyne detector about the x-axis.

6.4 Changing the PD Position on the Homodyne Detector

All previous data was taken with the PDs in Position 1 on the homodyne detector. After taking data with the two Rotational methods, the position of the PD was switched from Position 1 to Position 2 to confirm that this change had no effect on the DC Voltage Output. These configurations can be seen again in *Figure 7*. We then tested the LC #1 and #4 PDs with Rotation θ_y in this configuration.

6.5 Observations

It is important to note that as the process of taking data progressed, our method evolved and became more normalized. In the beginning, we would often adjust the scale to increase precision in our results; however, we noticed that changing the scale can alter the measurement. With such small differences between data points, we decided to keep the oscilloscope on the 50mV scale to have better accuracy in our readings. The oscilloscope would also raise the base voltage reading over a period of time. When we first turned on the oscilloscope, it would read at around 2mV with no light on the PD, but we discovered that after about ten minutes of ramp time, it would read around 9mV. We waited until the oscilloscope read 9mV with no light incident on the detector to begin taking data. We also learned that our setup could become uncalibrated easily. Because of this, we were careful to check that the homodyne detector was truly perpendicular at 0° on the rotational stage.

7 Results and Analysis

The results of the different experiments can be found in *Figures 13-14*. It is important to note that these graphs display the absolute value of the DC Voltage; however, the sign of the voltage is actually negative for PDs in position one and positive for the PDs in position two. The error in the data was calculated by watching the oscillation of the voltage reading for one minute. We

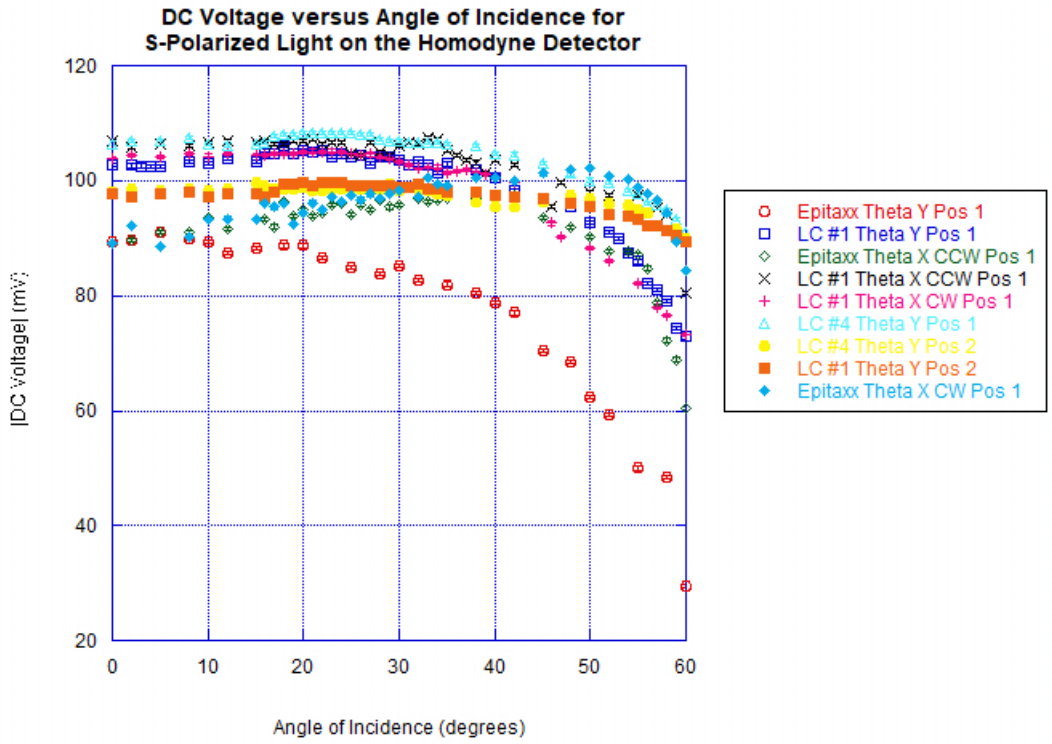

Figure 13: This figure shows the relationship between the DC Voltage Output and the AOI for all data where S-Polarized Light was incident on the PD. The various conditions under which each data set was taken are explained in the legend.

then took the highest and lowest values seen, subtracted them, and divided by two. This error can be seen in the error bars on each plot. All the raw data for this experiment can be accessed at: https://goo.gl/UfVgMo It seems that for all of the data sets, the homodyne detector shows a peak around 20°. The part we did not predict; however is that this maximum is not absolute for the P-Polarized Light. Also, we saw that the location of the maximum is slightly variable. To analyze these curves, we used "KaleidaGraph" to fit curves to the data sets depending on the polarization of the light used. For S-Polarized Light, we fitted the first portion of the data by the following equation:

$$y = M_0 + M_1 x + M_2 x^2$$

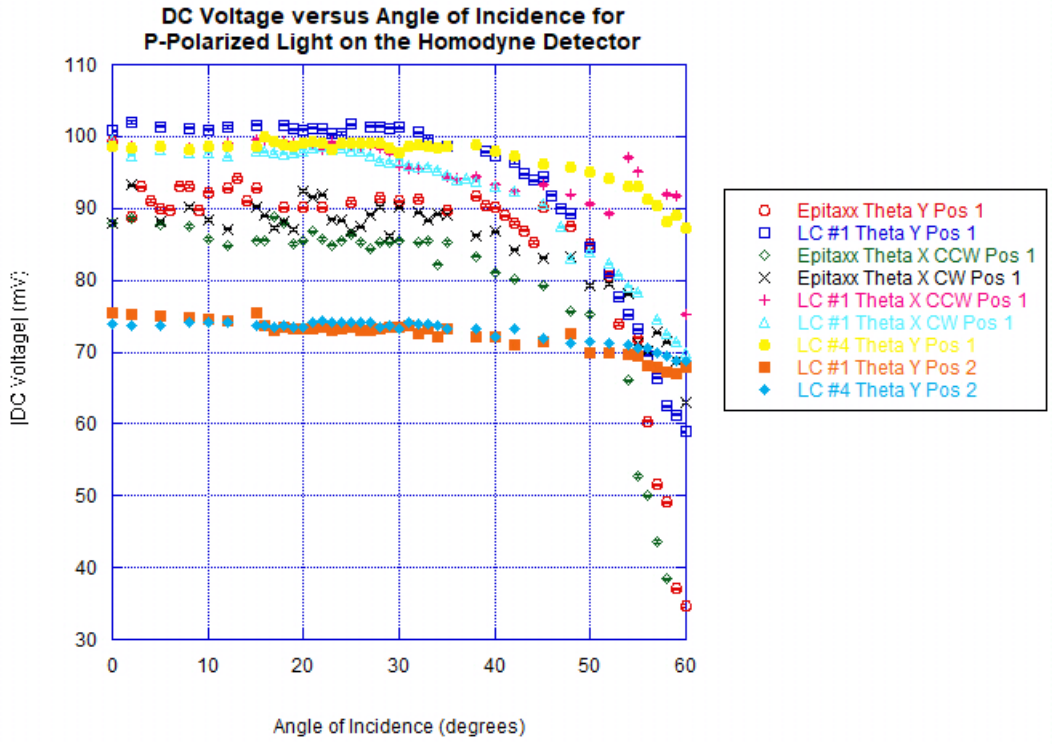

Figure 14: This figure shows the relationship between the DC Voltage Output and the AOI for all data where P-Polarized Light was incident on the PD. The various conditions under which each data set was taken are explained in the legend.

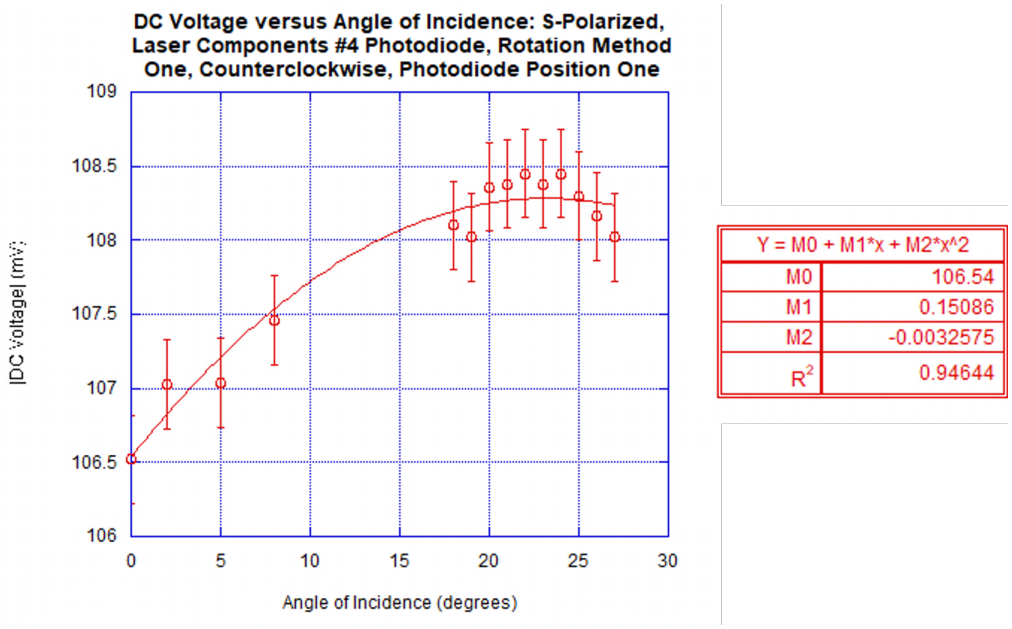

Figure 15: This figure shows the parabolic fit and equation applied to the first portion of the S-Polarized data taken with the LC #4 PD being rotated about the y-axis.

An example of this fit can be seen in *Figure 15*. The second half of the S-Polarization data as well as the entire P-Polarization curve were fitted with the following equation:

$$y = m_1 - m_2 e^{(m_3 x + m_4)}$$

Examples of these fits can be found in *Figures 16-17*.

After fitting the curves, for the S-Polarization, we calculated the maximum of the fit function for the first portion of the data to find the theoretical maximum DC Voltage and maximum AOI. We then compared the theoretical to the experimental with a percent difference. A summary of the S-Polarized Data can be found in *Figure 18*. For certain methods of rotation the fit is better than others. For the P-Polarized curve, we noticed that the first part of the function from an AOI of 0° to 25° was relatively constant. Because of this, to test the quality of our fit, we took the experimental average of the DC Voltage within that range as well as the average value of the function in the same range. We then compared the two vales through a percent difference

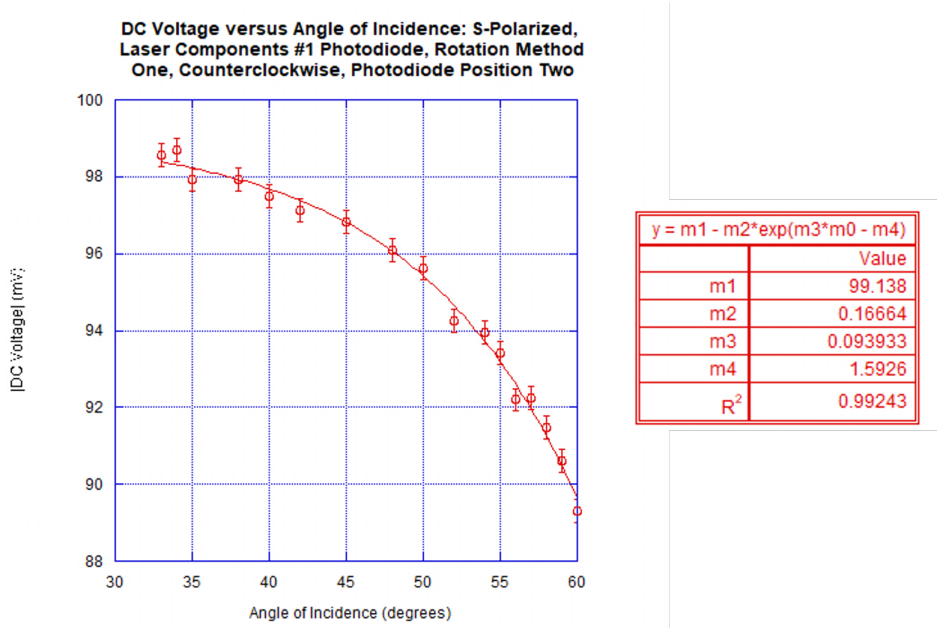

y = m1 - m2*exp(m3*m0 - m4)	
	Value
m1	99.138
m2	0.16664
m3	0.093933
m4	1.5926
R^2	0.99243

Figure 16: This figure shows the negative exponential grown fit and equation applied to the second portion of the S-Polarized data taken with the LC #1 PD being rotated around the y-axis in PD position two.

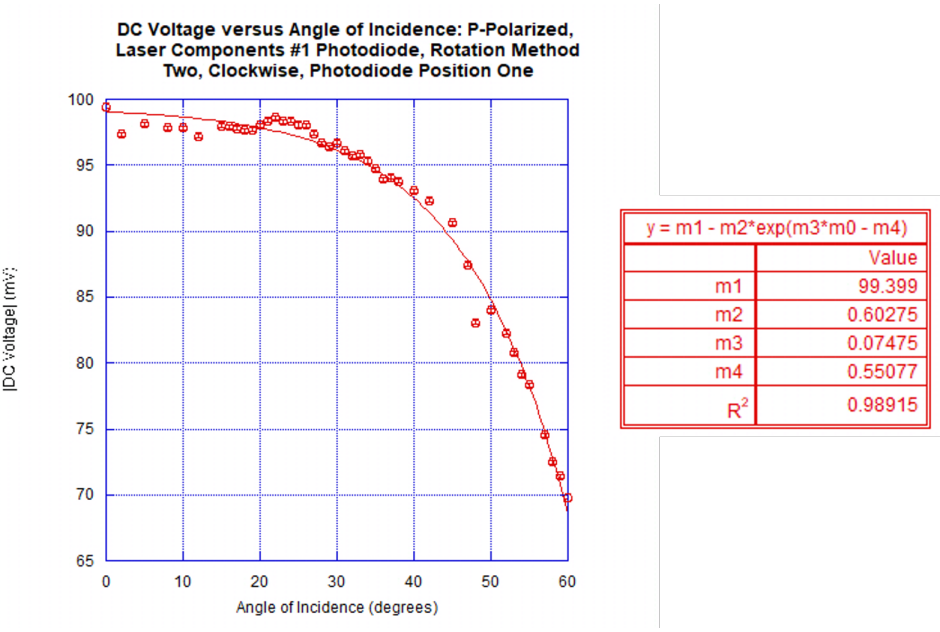

y = m1 - m2*exp(m3*m0 - m4)	
	Value
m1	99.399
m2	0.60275
m3	0.07475
m4	0.55077
R^2	0.98915

Figure 17: This figure shows the negative exponential growth fit and equation applied to the P-Polarized data for the data taken with the LC #1 PD being rotated about the x-axis in the clockwise direction.

Photodiode	Polarization	Rotation Method	Direction of Rotation	Photodiode Position	$\theta_{MAX\ (experimental)}$	DC $Voltage_{MAX\ (experimental)}$	$\theta_{MAX\ (from\ fit)}$	% difference	DC $Voltage_{MAX\ (from\ fit)}$	% difference
Epitax	S	θ_y	Counterclockwise	One	20°	88.7mV	5.90°	108.88%	89.75mV	1.18%
Epitax	S	θ_x	Counterclockwise	One	28°	96.53mV	65.30°	79.96%	98.94mV	2.47%
Epitax	S	θ_x	Clockwise	One	29°	97.82mV	65.50°	77.25%	102.36mV	4.54%
L.C. #1	S	θ_y	Counterclockwise	One	18°	106.02mV	20.00°	10.53%	104.65mV	1.30%
L.C. #1	S	θ_y	Counterclockwise	Two	23°	99.77mV	20.80°	10.05%	99.56mV	0.21%
L.C. #1	S	θ_x	Counterclockwise	One	21°	107.11mV	20.70°	1.44%	106.96mV	0.14%
L.C. #1	S	θ_x	Clockwise	One	23°	105.13mV	83.60°	113.70%	106.46mV	1.26%
L.C. #4	S	θ_y	Counterclockwise	One	22°	108.45mV	23.20°	5.31%	108.29mV	0.15%
L.C. #4	S	θ_y	Counterclockwise	Two	15°	99.76mV	17.50°	15.38%	98.6mV	1.17%

Avg $\theta_{MAX\ (experimental)}$	Avg DC $Voltage_{MAX\ (experimental)}$	Avg $\theta_{MAX\ (from\ fit)}$	% difference	Avg DC $Voltage_{MAX\ (from\ fit)}$	% difference
22.11°	101.03mV	35.83°	47.36%	101.73mV	0.69%

Figure 18: This figure summarizes all of the data taken with S-Polarized Light. We initially took the maximum AOI and DC Voltage from the experimental data and compared it to the maxima of the fitted functions through a percent difference calculation. After finding each value we averaged the experimental and theoretical values for the maximum AOI and DC Voltage and took and overall percent difference.

calculation; this is shown in *Figure 19*.

8 Conclusions and Perspectives

From the data, we have concluded that the Homodyne Detector in the Virgo Squeezing Lab does not need to be adjusted. It can remain in the setup with an AOI of 20°. The rotation will also remain about the y-axis. We found that the S and P-Polarized lights produce different curves. This shows that the polarization does have an effect on the DC Voltage produced by the PDs. For further research, we would like to take more data for each configuration. This will allow us to have more precise results. It would be especially helpful for the S-Polarized light to see if there is another possible cure fit for the first portion of the data. The ultimate goal would be to characterize all of the LC PDs.

Photodiode	Polarization	Rotation Method	Direction of Rotation	Photodiode Positon	Average DC Voltage$_{(experimental)}$	Average DC Voltage$_{(from\ fit)}$	% Difference
Epitax	P	θ_y	Counterclockwise	One	91.54mV	91.23mV	0.34%
Epitax	P	θ_x	Counterclockwise	One	86.24mV	86.00mV	0.28%
Epitax	P	θ_x	Clockwise	One	89.18mV	89.21mV	0.03%
L.C. #1	P	θ_y	Counterclockwise	One	101.18mV	101.83mV	0.64%
L.C. #1	P	θ_y	Counterclockwise	Two	73.89mV	74.20mV	0.42%
L.C. #1	P	θ_x	Counterclockwise	One	98.97mV	98.88mV	0.09%
L.C. #1	P	θ_x	Clockwise	One	97.94mV	98.38mV	0.45%
L.C. #4	P	θ_y	Counterclockwise	One	98.89mV	98.87mV	0.02%
L.C. #4	P	θ_y	Counterclockwise	Two	73.90mV	73.94mV	0.05%

Avg of Average DC Voltage$_{(experimental)}$	Avg of Average DC Voltage$_{(from\ fit)}$	% Difference
90.19mV	90.28mV	0.10%

Figure 19: This figure summarizes all of the data taken with S-Polarized Light. We initially took the average DC Voltage from the experimental data and compared it to the average value of the fitted functions through a percent difference calculation. After finding each value we averaged the experimental and theoretical values for the mean DC Voltage and took and overall percent difference.

9 Other Work at La Sapienza

Two of the projects being tackled by various faculty at La Sapienza are the Suspended Interferometer for Ponderomotive Squeezing (SIPS) Project and the assembly of payloads for Advanced Virgo (AdV). The SIPS project aims to create a system in which squeezed light can be produced using Ponderomotive techniques instead of Optical Parametric Oscillators. The payload assembly is a collaborative activity between INFN Roma One and many other institutions in Italy. The purpose is to assemble and suspend the payloads within Virgo. Sibilla Di Pace works mostly with the finite element analysis simulations to optimize the design of SIPS in order to be radiation pressure noise limited. Luca Naticchioni is the SIPS coordinator and works on payload assembly for AdV. Paola Puppo also assists with the payloads by running simulations to test thermal noise in these payloads. Ettore Majorana is an expert in in the control of suspension at Virgo and assists with the payload suspension to the super attenuator in Virgo.

Besides the experimental work being done at La Sapienza, there is also a large number of faculty working in a group to find Continuous GWs. This task is difficult because the signal duration of these waves is longer than those that have been observed in the past. An obvious source of continuous waves is asymmetric spinning neutron stars. Other possible sources include fast-spinning, young magnetars and super-radiant instabilities in spinning black holes. These occurrences, however, are hard to detect because often they do not know the typical amplitude of the signal. Another obstacle to consider is the changing position of the source which can cause amplitude and frequency modulation.

Cristiano Palomba is working in targeted searches for known pulsars. These searches are based on a match filter where the position, frequency, and spin-down of the star is known. This kind of search is the most specific out of the types of searches associated with continuous GWs. Simone Mastrogiovanni performs searches for poorly known neutron stars, so he works between direct and targeted searches. In direct searches, the position of the source is known, but the frequency and spin-down are not. He creates filters to deal with non-monochromatic signals due to the Doppler Effect, spin-down, and antenna response. With these filters he has characterized methods to look for continuous waves in Fermi-LAT data; however with the use of more templates, more outliars appear. These can be due to statistical fluctuation, Non-Gaussian data, and instrumental noise artifacts. Paola Leaci is investigating specifically continuous waves emitted by a companion orbiting a neutron star before coalescence. She observes accretion disks in low mass, x-ray binaries. The best candidate for her research is Scorpius X-1 because it is the brightest and closest of the low mass, x-ray binaries with the highest accuracy of orbit. When taking data, she wants to observe many orbits, so she tries to find binaries with smaller orbital periods. She has developed filters to look for Gaussian Noise characteristics in her data that may show information about orbit parameters and periodicity. Right now she is working to improve these filters for other sources of noise. One of the major components of this group is

Sergio Frasca. He has created a library of Band Sample Data or BSD that organizes the sample signals. With this library, there is a large amount of signals that are corrected for Doppler and spin-down and available for analysis. This allows for members of the group to have a well organized source of signals to use in their development of data analysis techniques.

10 Acknowledgments

I would like to thank the following people and institutions who helped make my work possible. Paola Puppo and Luca Naticchioni, thank you for taking me as a part of your team for the past two months. Sibilla Di Pace, thank you for being there to guide me through my project and to tell me anything I needed to know about my research, public transportation strikes, or Italian food. Thank you to La Sapienza for being an amazing host institution. Thank you to Bernard Whiting, Guido Miller, and the University of Florida for selecting me for this unique research opportunity, and thank you to the National Science Foundation for making it all possible. Finally, thank you to Andrew Miller for being my guide and translator for most of my time in Rome; I don't want to imagine having to survive here without you.

11 References

1. Albert Einstein Institut. (2017), Squeezed Light.

2. Advanced Virgo Squeezing Working Group. (2015), Advanced Virgo Squeezer Technical Design Report.

3. Di Pace, S. (2014), Towards the Observation of the Quantum Radiation Pressure Noise in a Susponded Interferometer: the QuRaG experiment.

4. Naticchioni, L. (2016), Ponderomotive squeezing of light; Overcoming the Standard Quantum Limit in the detection band of interferometric gravitational wave detectors.

5. Paschotta DRCBC. (2017), Gaussian Beams. Encyclopedia of Laser Physics and Technology - Gaussian beams, laser beam, fundamental transverse modes. RP Photonics Consulting GmbH.

6. Sequino V, Vardaro M, et al. (2017), Development of an audio-frequency band vacuum squeezer for the quantum noise reduction in the Gravitational Wave detector Advanced Virgo.

7. LIGO IPAC Communications Education Team. (2014) What are Gravitational Waves?.

12 Appendix I

Experimental Equipment

1. Thorlabs 125mm Lens
2. Thorlabs 200mm Lens
3. Polarizing Beam-Splitter
4. Two Thorlabs Quarter Wave Plate Polarizers
5. Three Thorlabs Linear Translation Stages
6. Thorlabs 1-Aixis Rotation Stage
7. Various Thorlabs Mounts
8. Optical Filter
9. InnoLight Nd:YAG Infrared Laser 1064nm
10. Homodyne Detector Circuit Board developed by the Advanced Virgo Squeezing Group at La Sapienza
11. Eptiaxx PD
12. LASER COMPONENTS #1 PD
13. LASER COMPONENTS #4 PD
14. IsoTech Laboratory DC Power Supply
15. Keysight InfiniiVision Digital Storage Oscilloscope
16. LaserPoint Mod 3000-Laser Power and Energy Meter
17. 2.1 Andover Corporation Optical Density